Vienna Congress on Recent Advances in
Earthquake Engineering and Structural Dynamics 2013 (VEESD 2013)
C. Adam, R. Heuer, W. Lenhardt & C. Schranz (eds)
28-30 August 2013, Vienna, Austria
Paper No. 218

Plastic hinge models for the displacement-based assessment of wall-type bridge piers with poor detailing

P. Hannewald[1], K. Beyer[1]

[1] Earthquake Engineering and Structural Dynamics Laboratory (EESD), School of Architecture, Civil and Environmental Engineering (ENAC), École Polytechnique Fédérale de Lausanne (EPFL), Switzerland

Abstract. This paper presents a plastic hinge modelling approach for wall-type bridge piers with detailing deficiencies such as low transverse reinforcement ratios and lap splices in potential plastic hinge regions. Currently available plastic hinge length estimates and strain limits are validated against a series of seven large scale tests, representing poorly detailed bridge piers. Besides the flexural deformations, which are predicted with the plastic hinge approach, the shear deformations need to be taken into account due to the geometry and detailing of the considered piers. Shear-flexure interaction is accounted for by relating the shear distortion to the axial strains in the plastic hinge. Lap splices in potential plastic hinge regions have a significant influence on the displacement capacity of the structure as their degradation may lead to a nearly instant loss of lateral load bearing capacity. Hence, strain limits defining the onset of splice degradation are assessed using the experimental data.

Keywords: Plastic hinge; Wall-type piers; Detailing deficiencies; Lap-splices; Displacement-based assessment

1 INTRODUCTION

Many bridges in Switzerland were built before modern seismic design provisions were introduced in design codes. Many of these bridges feature wall-type reinforced concrete (RC) piers that are prone to brittle shear failure under seismic loading if poorly detailed. Common detailing of these piers includes low transverse reinforcement ratios and a lack of confining reinforcement, which leads potentially to a non-ductile performance of the structure. Moreover, to facilitate construction, the longitudinal reinforcement is typically spliced right above the foundation of the pier, where a plastic hinge may develop. Retrofitting all bridges with the mentioned deficiencies to ensure a ductile behaviour when subjected to seismic loading or withstand the expected force demands in the elastic regime would be uneconomical. Instead, since the level of seismic hazard in Switzerland is only moderate, the displacement-capacity of these bridges should be assessed. However, easily applicable models with which the displacement capacity can efficiently be predicted are necessary in light of the large Swiss bridge stock. Even though the research presented in this paper stems from the need to establish such a modelling approach for the assessment of Swiss bridges, the situation is similar in other countries of moderate seismicity, where a significant amount of existing structures may not comply with modern seismic design requirements.

This paper presents a plastic hinge modelling approach with which the force-displacement response of poorly detailed wall-type piers can be estimated. It is validated against a test series of seven large scale tests on such piers constructed with typical detailing deficiencies. Due to the geometry and the detailing of the reinforcement, shear deformations constitute a significant part of the total deformation for this type of piers and must hence be considered in the prediction of the force-displacement response. Furthermore, the influence of lap splices in the plastic zone above the pier base must be

taken into account. The shear-flexure interaction is incorporated in the modelling approach by estimating the shear deformations as a function of the axial strains expected in the plastic hinge region. To account for the effect of the lap splices on the force-deformation behaviour, strain limits which define the curvature at which the onset of splice degradation is expected are employed. Firstly, the test series used for validation is introduced and some of the main results, which are needed for comparison with the model, are presented.

2 EXPERIMENTAL DATABASE

2.1 Overview of experimental campaign

A series of seven large scale tests conducted at ETH Zurich, Switzerland (VK1-VK3: Bimschas 2010, VK4-VK7: Hannewald et al. 2013) is used for the validation of the plastic hinge modelling approach. The test units were constructed with detailing that represents the commonly found deficiencies in existing bridge piers in Switzerland. To identify a critical pier layout that represents actual construction practice, Bimschas (2010) evaluated the detailing and geometry of existing bridge structures. An intermediate aspect ratio, for which neither pure flexural behaviour nor a load transfer through direct strut action was expected, was deemed potentially shear critical. Furthermore, a small amount of stirrups that were not anchored in the concrete core was provided, according to common construction practice in the past, and the longitudinal reinforcement was not confined. Three out of the seven piers were constructed with lap splices in the longitudinal reinforcement right above the foundation. Their length corresponds to the minimum length that was required by the Swiss codes (SIA 162 1968) for splices with straight bars that are not subject to tension. It should thus constitute a lower bound for the splice lengths that are found in existing Swiss bridge piers.

All piers had the same rectangular cross section with longitudinal reinforcement of diameter d_l=14 mm that was evenly distributed along the circumference of the section. Steel type "topar S500" of ductility class C with a yield strength of 521 MPa (VK1-VK3: 515 MPa) was used for the longitudinal reinforcement and cold formed steel with an equivalent yield strength of 528 MPa (VK1-VK3: 518 MPa) for the transverse reinforcement. Further material properties and characteristics of the test units are provided in Table 1.

Table 1. Overview of analysed test units (Bimschas 2010, Hannewald et al. 2013)

Test unit	VK1	VK2	VK3	VK4	VK5	VK6	VK7
Shear span L_s [m]	3.30	3.30	3.30	3.30	4.50	4.50	3.30
Aspect ratio L_s/l_w [-]	2.20	2.20	2.20	2.20	3.0	3.0	2.20
Concrete strength f_c [MPa]	35.0	39.0	34.0	34.6	35.2	44.4	30.0
Axial load ratio $n=P/(b\ l_w f_c)$	0.064	0.071	0.073	0.072	0.070	0.056	0.083
Longitudinal / transverse reinforcement ratio [%]	0.82 / 0.08	0.82 / 0.08	1.23 / 0.08	1.23 / 0.08	1.23 / 0.08	1.23 / 0.08	1.23 / 0.22
Lap splice length l_s	-	$43d_l$	-	$43d_l$	$43d_l$	-	-

A cyclic load history with two cycles at each load level and small intermediate cycles in the inelastic range was applied. The axial load was kept constant throughout the test. The elongation of the wall along the narrow faces was measured with LVDTs and the in-plane deformations of the wall surface were measured along a square grid of Demec or LED targets, respectively. In the following section, the results required for evaluating the performance of the plastic hinge model will be presented. For further results and information on the tests, the reader is referred to Bimschas (2010) and Hannewald et al. (2013).

2.2 Results

Besides the force-displacement response of the pier, the flexural and shear deformation components as well as the maximum strains at the bottom of the pier are of interest for the validation of the plastic hinge model. Figure 1a shows the backbone curves of the force-displacement response of all seven test units which were constructed from the first cycles in the positive loading direction. One can note that up to the peak response, the force-displacement response of the test units with spliced reinforcement (plotted with hollow markers) are almost equal to the corresponding ones with continuous reinforcement (plotted with filled markers). At the peak response, the degradation of the lap splice and thus the degradation of the shear resistance initiates. Generally, the resistance of the units with splices is degrading much faster from then on, except for the pair VK3 & VK4. Test unit VK3, which did not feature a lap slice, degrades with about the same rate at a slightly higher drift due to a relatively brittle shear failure mode. However, the residual resistance of these two test units and that of all other corresponding pairs differs. While the end of the plotted response marks the axial failure of all test units with continuous reinforcement, the tests of the piers with the lap splices were stopped when the lateral resistance hardly degraded further. From then on, the lateral resistance stemmed from the eccentricity of the axial force, which the piers were still able to sustain.

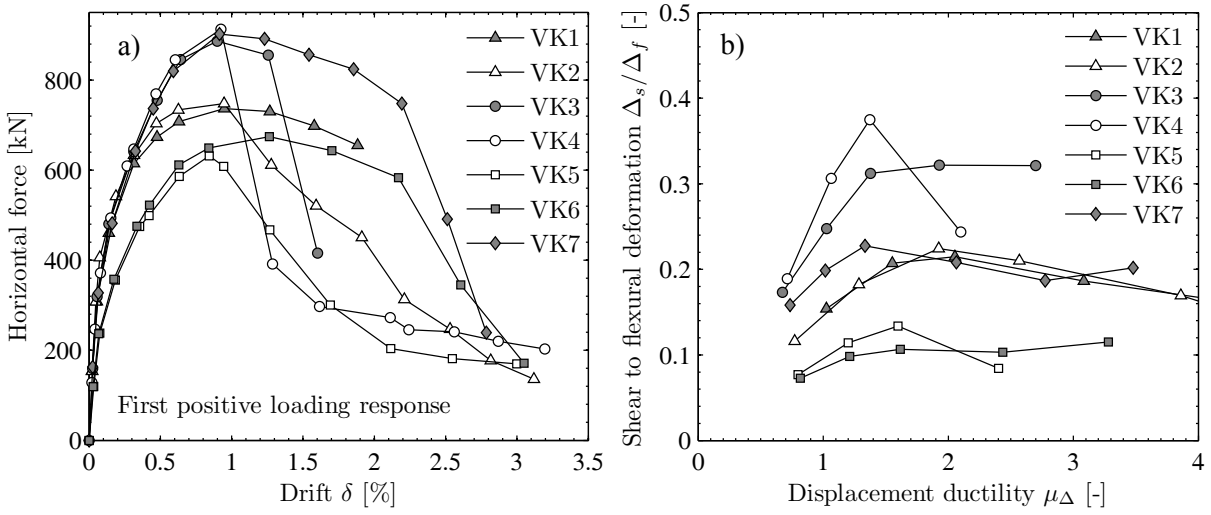

Figure 1. Force-displacement response and shear to flexure ratios of considered test units

Besides the force-displacement response, Figure 1 also shows the average shear to flexural deformation ratios obtained from the measurements at the peak displacements of each cycle in positive and negative loading direction. Both deformation components in this plot were calculated from Demec (VK1-3) and optical measurements (VK4-7), respectively. The shear deformation contains base-sliding deformation and the flexural deformation contains fixed-end rotation due to strain penetration. As it is assumed that the ratios will be related in the inelastic range, where they have been previously observed to be approximately constant for flexure controlled walls (e.g. Dazio et al. 2009), the ratios are here plotted for displacement ductilities larger than $\mu_\Delta \approx 1.0$. The plot shows that the ratios of the slender test units VK5 & VK6 are indeed approximately constant whereas this does not apply to the other walls. Furthermore, it is also evident that shear deformations can constitute a significant part of the total deformation, especially if the transverse reinforcement ratio and slenderness are not high.

3 FLEXURAL DEFORMATION

3.1 Computation of flexural deformation

The plastic hinge modelling approach is based on integration of a simplified curvature profile and hence employable to predict the flexural deformations of a structure. The curvature profile is

simplified in the sense that the inelastic curvature profile, which increases towards the base, is replaced by a curvature profile that comprises a constant curvature along the plastic hinge length. Above the plastic hinge, only elastic deformations are assumed to occur. This simplified treatment allows for an easy integration of the curvature as well as for estimating the post-peak response of a member. The quality of the prediction made with the plastic hinge approach strongly depends on the chosen plastic hinge length and the moment-curvature analysis used to calculate the base curvatures. Previously, the plastic hinge length L_p suggested by Bohl and Adebar (2011) was identified to yield good results for the walls investigated here, see Hannewald and Beyer (2012). This L_p was established based on the results of a numerical study on walls with varying cross section and aspect ratio:

$$L_p = (0.2l_w + 0.05L_s)(1 - 1.5n) \leq 0.8l_w \tag{1}$$

where L_s and l_w are the shear span and the wall length, respectively, and n is the axial load ratio. To validate the choice of the plastic hinge length, an estimate of L_p can be calculated using the experimental data following a procedure suggested by Hines et al. (2004). According to this, L_p can be calculated from the experimentally determined plastic flexural deformation as follows:

$$L_p = \frac{\Delta_{p,fl}}{\phi_p L_s} \tag{2}$$

In this equation, ϕ_p is the plastic base curvature, which is not directly obtained from measurements but from extrapolation of the linearly approximated inelastic part of the curvature profile to the wall base. Thereby one obtains the total base curvature ϕ_b, from which the elastic curvature can be subtracted to obtain the plastic curvature. This procedure provides an approximate correction of the curvature for strain penetration effects. The difference between the extrapolated curvature and the curvature obtained from the readings of the measurement devices covering the basecrack, $\phi_{b,m}$, is interpreted as strain penetration influence. The strain penetration is hence included in the plastic hinge length itself and no additional fixed end rotation component needs to be considered to account for its influence.

If the plastic hinge length is known, the flexural deformation can be computed according to a formulation suggested by Priestley et al. (2007), with which the entire load-deformation curve can be predicted:

$$\Delta'_y = \frac{\phi'_y L_s^2}{3} \qquad \text{for } \phi \leq \phi'_y \tag{3a}$$

$$\Delta = \Delta'_y \frac{M}{M'_y} + \left(\phi - \phi'_y \frac{M}{M'_y}\right) L_p L_s \qquad \text{for } \phi > \phi'_y \tag{3b}$$

where ϕ'_y and M'_y are the curvature and corresponding moment at which the yield strain of the outer longitudinal reinforcement bars or a concrete peak compression strain of $\varepsilon_c = 0.002$ is reached, whichever occurs first. The above equation does not include the strain penetration length at yield displacement, which was included in the original formulation of the equation. All curvatures and corresponding moments are computed using a fibre-section analysis. For the one used in here, the confined concrete model according to Mander et al. (1988) and a bilinear stress-strain relationship for steel, including strain hardening, were used. Tension stiffening was not considered.

3.2 Strain and curvature limits

Usually, the displacement capacity of a structure is limited by local damage such as crushing of concrete, buckling or rupture of the reinforcing bars. Hence, strain limits, which indicate when the mentioned failure modes are expected to occur, are defined and used in conjunction with moment curvature analysis. In this study, proposals of strain limits by two different groups of researchers have been examined. Both suggest a limit strain for concrete as well as for steel for the failure modes

indicated in the respective paragraphs below, but since the concrete strains were decisive for the examined walls, only those are reported here for brevity. Priestley et al. (2007) suggest a "damage control compression strain" which indicates when the confining reinforcement is expected to rupture. It was derived based on the assumption that the ultimate strain of unconfined concrete can be estimated as $\varepsilon_c = 0.004$ using the confined concrete model by Mander et al. (1988). Equating the post-peak strain energy of concrete with the strain energy of the reinforcement before rupture yields the following expression:

$$\varepsilon_{cu} = 0.004 + 1.4\frac{\rho_v f_{yv} \varepsilon_{su}}{f_{cc}} \tag{4}$$

where ρ_v, f_{yv} and ε_{su} are the ratio, yield strength and ultimate strain of the transverse reinforcement, respectively, and f_{cc} is the confined concrete strength. Biskinis and Fardis (2010) used a comprehensive experimental database and considered the measured drifts at which the lateral resistance had dropped by 20% to deduce a strain limit. This strain limit does hence not define a local damage state, but is directly related to a global measure, i.e. the reduced shear capacity. Besides the effect of the confinement, the observation that the size of the confined area in compression has an influence is taken into account in their equation:

$$\varepsilon_{cu} = 0.0035 + \left(\frac{1}{x_{c,con}}\right)^{1.5} + 0.4\frac{k_{con}\rho_v f_{yv}}{f_{cc}} \tag{5}$$

where $x_{c,con}$ is the depth of the confined part of the compression zone and k_{con} is a confinement effectiveness factor according to Sheikh and Uzumeri (1982), taking into account the spacing of the reinforcement in relation to the dimensions of the cross section. Kazaz et al. (2012) chose a different approach to obtain a limit measure for the ultimate state: Instead of strain limits, curvature limits were defined. These were obtained from strains of numerical models of a large set of walls. The curvatures were determined when the lateral load capacity of the model had either dropped by 15%, a maximum compression strain that caused spalling of concrete was reached or the maximum steel strain was 10%. A regression analysis on the curvatures which were obtained for these limit states for the walls with varying parameters, yielded the following expression for the limit curvature of rectangular walls subjected to cyclic loading:

$$\phi_u = \frac{0.8 \cdot 0.75 \cdot 1.0}{l_w}\varepsilon_{su}\,(1 - 2.4n)\left(1 - 1.5\,\frac{f_{yv}\rho_v}{f_c}\right)\left(\frac{L_s}{l_w}\right)^{0.29} \tag{6}$$

Table 2 summarises the limit strains and curvatures according to Equations (4) – (6) for the test units with continuous reinforcement. Limit strains for test units with lap splices will be treated in Section 5.1.

Table 2. Strain and curvature limits defining the displacement capacity

Test unit	VK1	VK3	VK6	VK7
Equation (4) $\varepsilon_{cu,1}$ [‰]	5.39	5.43	4.95	7.85
Equation (5) $\varepsilon_{cu,2}$ [‰]	4.84	4.80	4.62	8.57
Equation (6) ϕ_u [1/m]	0.0517	0.0513	0.0517	0.0418

3.3 Discussion of results

Firstly, the quality of the plastic hinge length prediction is examined. To this end, the predicted length is compared to the one derived from the experimental data, as shown in Figure 2a. The experimental plastic hinge length was evaluated according to Equation (2) as outlined in the previous section. The difference between the extrapolated base curvature and the first yield curvature ϕ'_y according to

moment curvature analysis was taken as the plastic base curvature in Eq. (2). By doing so, a plastic hinge length that provides the best link between the analytical curvature at first yield ϕ'_y and the measured top displacement in the inelastic range is obtained. This is well comparable to the predicted plastic hinge lengths, which will be used to estimate a top displacement based on an analytical estimate of ϕ'_y. Figure 2a shows that, even though Equation (1) does not contain a strain penetration component, it provides a satisfactory estimate of the average experimental plastic hinge length of each test unit that was not corrected for strain penetration influence. The range of predicted plastic hinge lengths is shaded in grey with the lower and upper bound corresponding to the lowest and highest aspect ratio, respectively. Figure 2b shows that with this plastic hinge length and Equation (3) the flexural deformation is generally well predicted. In the predictions, the attainment of the limit strains and curvature according to Equation (4) ($\varepsilon_{cu,1}$), Equation (5) ($\varepsilon_{cu,2}$) and Equation (6) (ϕ_u) is marked. One can note that generally the strain limits correspond to a state right after the peak response. The values proposed for limit curvatures on the other hand correspond to large deformations which have not been reached in the experiments. This might be due to the fact that ϕ_u has been developed for walls with well confined boundary elements, whose resistance decreases to 85% of the peak value only at large ductility demands.

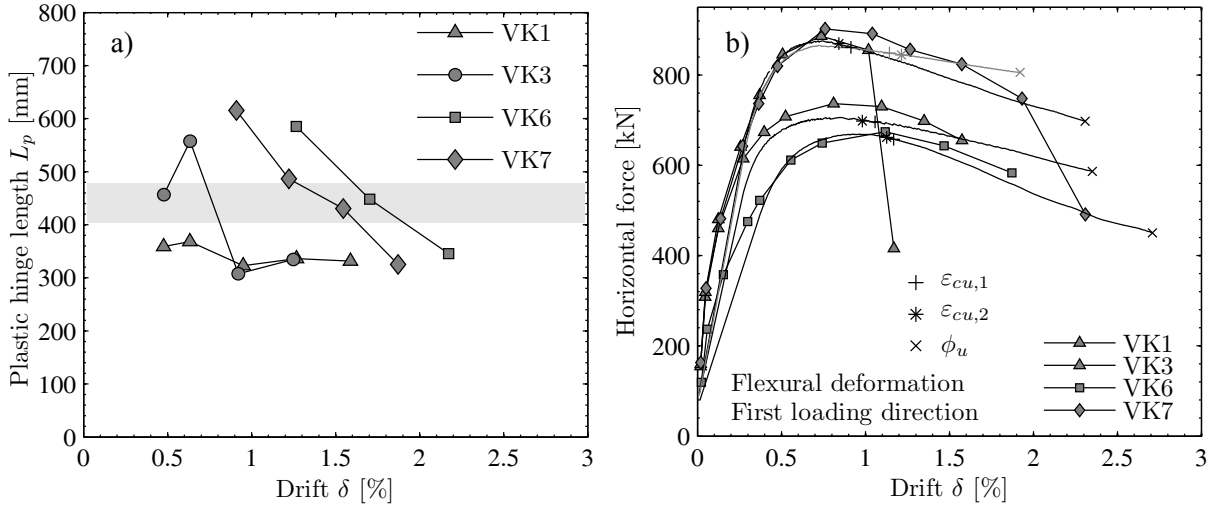

Figure 2. Predicted plastic hinge lengths (shaded in grey) and predicted flexural response compared to experimental data.

4 SHEAR DEFORMATION

Since shear deformations constitute a significant portion of the total displacements (Figure 1b), they must be incorporated in the plastic hinge modelling approach. Shear-flexure interaction is accounted for through a relation between flexural deformations Δ_f and shear deformations Δ_s proposed by Beyer et al. (2011). In this approach, the ratio Δ_s/Δ_f is estimated as a function of the centroidal axial strain in the plastic hinge, which can be obtained from moment-curvature analysis. Besides the strains, the minimum angle of the shear cracks relative to the element axis θ is necessary to relate the axial strain to the shear distortion according to Mohr's circle. With the assumptions that the remaining strain components adding to shear distortion are negligible and that shear deformations mainly occur in the plastic hinge, the shear to flexural deformation ratio results as:

$$\frac{\Delta_s}{\Delta_f} = \alpha \frac{\varepsilon_x}{\phi \tan\theta} \frac{1}{L_s} \tag{7}$$

where α is a correction factor. As evident in Figure 1b, the ratio Δ_s/Δ_f is not constant for the examined walls, which were not purely flexure controlled. The figure also shows that Δ_s/Δ_f decreases with the slenderness of the wall and increasing transverse reinforcement ratio. To take into account the latter and the general observation that walls with lower shear strengths have larger shear deformations, Hines et al. (2004) proposed the following correction factor:

$$1.0 \leq \alpha = \frac{V}{V_{UCSD}} + \frac{V}{V_{wc}} \leq 2.0 \tag{8}$$

where V_{UCSD} is the shear strength proposed by Kowalsky and Priestley (2000) which is regarded to be a measure for the diagonal tensile strength and V_{wc} is the web crushing strength. To compute the latter, the formulation for the compression strut capacity according Eurocode 2 (2004) was used. Equations (7) and (8) were used to calculate the ratio of shear to flexural deformation of each test unit for all inelastic top displacements based on the corresponding curvature and strain according to moment curvature analysis. To evaluate Equation (7), the axial strain and curvature corresponding to the maximum moment according to the moment curvature analysis were used and the crack angles were measured from photographs. Figure 3 compares the predictions to the experimentally determined Δ_s/Δ_f -ratios at peak load in positive and negative loading direction. One can see that the ratios are predicted reasonably well, also in light of the scatter associated with the experimental results.

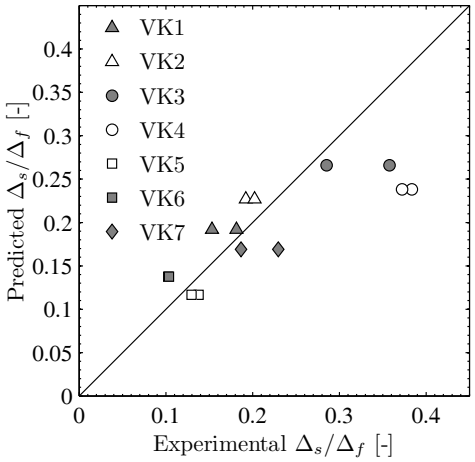

Figure 3. Predicted Δ_s/Δ_f ratios at peak load compared to experimental ones.

5 LAP SPLICES

5.1 Failure limit strains

As outlined in Section 2 and shown in Figure 1a, the test units which were constructed with spliced reinforcement at the base showed the same behaviour as those without splices up to the point at which degradation of the splice set in. From this point onwards, a rapid degradation of the resistance was observed. Hence, to predict the force-displacement response of piers with lap splices, strain limits defining the onset of lap splice degradation are required.

Priestley et al. (1996) argue that, if the splice is not well confined, its capacity under cyclic loading begins to drop when the confining concrete first cracks in compression. This limits the ability of the concrete to transfer the force from one bar to another after load reversal when the splice is in tension. Thus, Priestley et al. suggest to limit the concrete compression strain to ε_c=0.002, corresponding to the strain at peak concrete strength. Biskinis and Fardis (2010) suggest a strain limit for the steel in

tension, which is a fraction of the limit strain proposed for continuous reinforcement related to the length of the splice:

$$\varepsilon_{su,s} = \left(1.2\frac{l_s}{l_{su,min}} - 0.2\right)\frac{3}{8}\,\varepsilon_{su} \tag{9a}$$

$$l_{su,min} = \frac{d_l f_{sy}}{1.05+14.5\left(1-\frac{0.5s}{h_{con}}\right)\left(1-\frac{0.5s}{b_{con}}\right)\frac{n_{res}}{n_l}\frac{\rho_v f_{yv}}{f_c}\sqrt{f_c}} \tag{9a}$$

where $l_{su,min}$ is the minimum splice length required for cyclic loading, which depends on the confinement conditions. The latter is taken into account through the transverse reinforcement ratio ρ_v, the number of restrained splices in relation to the number of total splices, n_{res}/n_l and the dimensions of the confined core, h_{con} and b_{con}. No compression strain limit which is explicitly derived for members with spliced reinforcement is provided. This leads to the conclusion that no refinement of the concrete limit strain was necessary and Equation (5), which defines the limit strain of concrete for members with continuous reinforcement, is still valid.

Table 3. Strain and curvature limits for the onset of splice degradation

Test unit	VK2	VK4	VK5
Priestley et al. ε_c [‰]	2.00	2.00	2.00
Equation (5) ε_c [‰]	4.78	4.80	4.78
Equation (9a) ε_s [‰]	22.9	18.2	18.4
Equation (9b) $l_{su,min}$ [mm]	1051	1122	1113

5.2 Discussion of results

For each of the examined wall sections, the concrete limit strain was decisive because, according to the results of moment-curvature analyses, it was reached just prior to the steel limit strain. This corresponds well to the test results. Degradation of the lap splices of both VK2 and VK4 initiated when the concrete was crushed in compression at the outer edge of the section. Only the splice of VK5 began to fail due to tensile splitting at the load step prior to the one for which damage of the concrete was expected in compression.

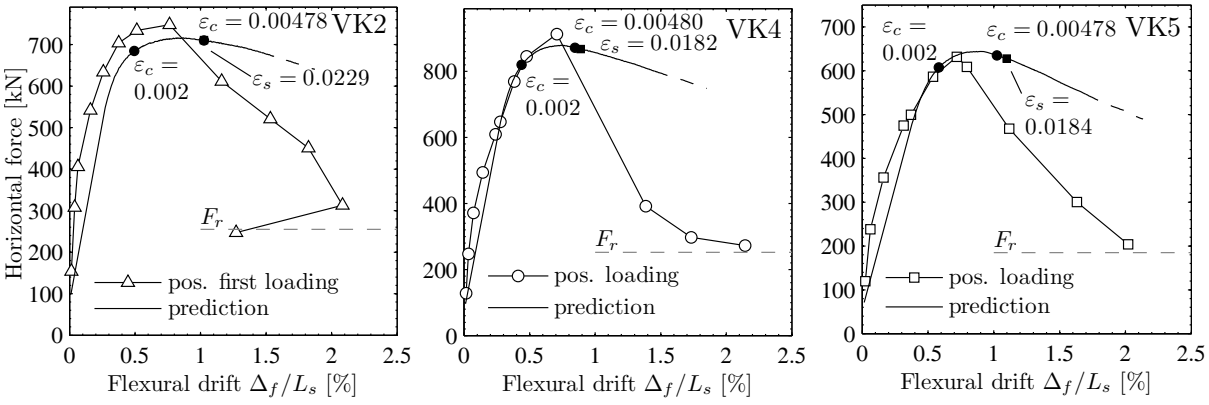

Figure 4. Comparison of predicted and measured flexural responses of the test units with lap splices.

Figure 4 shows the flexural response predicted for the test units with spliced reinforcement in comparison to the measured ones. The points at which the previously introduced concrete and steel limit strains are reached in the analysis are marked in each plot. All plots show that the lowest concrete strain limit of ε_c=0.002 provides a very conservative limit for the onset of splice degradation. The confined concrete strain limit on the other hand is reached just before the splice starts degrading

in case of VK2 and VK4, while it slightly overestimates the drift capacity of VK5. But, as VK5 did not degrade due to concrete crushing, this could be expected. With the concrete strain according to Equation (5) on the contrary, the drift at which splice failure occurs is slightly overestimated. The limit strain for the steel is reached at about the same curvature as the concrete limit strain (VK2) or at a higher curvature (VK4 & VK6) and hence not decisive here.

As degradation progresses very rapidly once it was initiated, it is deemed reasonable to assume that the lateral load capacity will immediately drop to a residual value. This residual value depends on the maximum eccentricity of the axial load within the confined section and is indicated with a dashed line in Figure 4. Comparison with Figure 1a shows that the resistance actually continues to decrease a bit further, as the concrete within the confined area is increasingly crushed which reduces the eccentricity of the axial load. However, for modelling purposes, the simplifying assumption that the resistance immediately drops to a constant residual value once the concrete limit strain is reached may be made.

6 CONCLUSIONS

In this paper, a plastic hinge modelling approach that is applicable to wall-type piers with structural deficiencies is defined and validated against a series of seven large scale tests. It is shown that the flexural deformations can be well predicted with the plastic hinge length estimates for structural walls suggested by Bohl and Adebar (2011) in combination with a refined modelling approach proposed by Priestley et al. (2007). Currently available strain limits yield deformation capacities that correspond approximately to the peak-strength of a structureand are hence somewhat conservative. However, in light of the fact that the walls may exhibit brittle shear failure at slightly larger drifts, these conservative strain limits may be considered as reasonable estimates of the drift capacity.

The prediction of the shear deformation is associated with a larger variation than the flexural deformation. Nevertheless, satisfactory results are obtained with the approach suggested by Beyer et al. (2011), if the increased shear deformation of piers with low transverse reinforcement, and hence low diagonal tensile strength, is taken into account. To improve the shear deformation predictions, further investigations will be made using a larger database of shear walls. The reduced drift capacity of piers with spliced reinforcement could be estimated using the concrete limit strain by Biskinis and Fardis (20110). However, especially the drift of the pier whose capacity dropped before the concrete was crushed in compression was slightly overestimated with this limit. Experimental research is currently underway to examine the behaviour of splices under reversed cyclic loading in more detail with the aim to investigate which loading conditions and strains might, besides a large concrete compression strain, trigger splice failure, see Angeli et al. (2013). Furthermore, strain limits for the concrete will be investigated in more detail. Based on the test data considered here, it is recommended to assume an immediate drop of capacity to the residual capacity determined by the eccentricity of the axial load.

ACKNOWLEDGEMENTS

The study presented in this paper has been carried out in the framework of a research project funded by the Swiss Federal Roads Office (FEDRO) with project number AGB 2008/001. This financial support is gratefully acknowledged.

REFERENCES

Angeli, G., Hannewald, P. and Beyer, K. (2013). Check title. *Proceedings of the xx VEESD,* August …x. 2013, Vienna, Austria, Paper No. xxx

Beyer, K., Dazio, A. and Priestley, M.J.N. (2011). Shear deformations of slender RC walls under seismic loading. *ACI Structural Journal*, **108**, 167-177.

Bimschas, M. (2010). *Displacement-Based Seismic Assessment of Existing Bridges in Regions of Moderate Seismicity*, IBK Report 326, Swiss Federal Institute of Technology ETH, Zurich, Switzerland

Biskinis, D. and Fardis, M.N. (2010). Flexure-controlled ultimate deformations of members with continuous or lap-spliced bars. *Structural concrete*, **11**, 93-108.

Bohl, P. and Adebar, P. (2011). Plastic hinge lengths in high-rise concrete shear walls. *ACI Structural Journal*, **108**, 148-157.

Dazio, A., Beyer K. and Bachmann, H. (2009). Quasi-static cyclic tests and plastic hinge analysis of RC structural walls. *Engineering Structures*, **31**, 1556-1571.

Eurocode 2 (2004). *Design of concrete structures: Part 1-1: General rules and rules for buildings.* Building code, European Committee for Standardization, Brussels, Belgium.

Hannewald, P. and Beyer, K. (2012). Plastic hinge models for the seismic assessment of reinforced concrete wall-type piers with detailing deficiencies. *Proceedings of the 15th World Conference on Earthquake Engineering*, September 24- 28, 2012, Lisbon, Portugal, Paper No. 1457

Hannewald, P., Bimschas, M. and Dazio, A. (2013). *To be published: Quasi-static cyclic tests on RC bridge piers with detailing deficiencies*, IBK Report, Swiss Federal Institute of Technology ETH, Zurich, Switzerland

Hines, E., Restrepo, J. and Seible, F. (2004). Force-displacement characterization of well-confined bridge piers. *ACI Structural Journal* **101**, 537-548.

Kazaz İ., Gülkan, P. and Yakut, A. (2012) Deformation limits for structural walls with confined boundaries. *Earthquake Spectra*, **28**, 1019 – 1046.

Kowalsky, M.J. and Priestley, M.J.N. (2000) Improved analytical model for shear strength of circular reinforced concrete columns in seismic regions. *ACI Structural Journal*, **97**, 388–396.

Mander, J.B., Priestley, M.J.N, and Park, R. (1988). Theoretical stress-strain model for confined concrete. *ASCE Journal of Structural Engineering*, **114**, 1804–1826.

Priestley, M.J.N, Calvi,G.M. and Kowalsky,M.J. (2007) *Displacement based seismic design of structures*. IUSS Press, Pavia, Italy.

Priestley, M.J.N., Seible, F. and Calvi, G.M. (1996) *Seismic design and retrofit of bridges*. John Wiley & Sons, Inc., New York, NY.

SIA 162 (1968) *Norm für die Berechnung, Konstruktion und Ausführung von Bauwerken aus Beton, Stahlbeton und Spannbeton (Code for the calculation, construction and execution of concrete, reinforced concrete and prestressed concrete structures)*, Swiss Societey of Engineers and Architects, Zurich, Switzerland

Sheikh, S.A. and Uzumeri, S.M. (1982) Analytical model for concrete confinement in tied columns. *Journal of the Structural Division*, **108**, 2703–2722.